C. R. Mecanique 345 (2017) 378–385

Contents lists available at ScienceDirect

Comptes Rendus Mecanique

www.sciencedirect.com

Optimal streaks in the wake of a blunt-based axisymmetric bluff body and their influence on vortex shedding

Mathieu Marant [a], Carlo Cossu [a], Grégory Pujals [b]

[a] Institut de mécanique des fluides de Toulouse, CNRS–INP–UPS, 2, allée du Professeur-Camille-Soula, 31400 Toulouse, France
[b] PSA Peugeot Citroën, Centre technique de Vélizy, 2, route de Gisy, 78943 Vélizy-Villacoublay cedex, France

ARTICLE INFO

Article history:
Received 3 February 2017
Accepted 11 May 2017
Available online 7 June 2017

Keywords:
Fluid dynamics
Hydrodynamic stability
Flow control

ABSTRACT

We compute the optimal perturbations of azimuthal wavenumber m THAT maximize the spatial energy growth in the wake of a blunt-based axisymmetric bluff body. Optimal perturbations with $m \neq 0$ lead to the amplification of streamwise streaks in the wake. When forced with finite amplitude $m \neq 1$, optimal perturbations have a stabilizing effect on large-scale unsteady vortex shedding in the wake. We show that $m \geq 2$ modes, which are forced with zero mass flux, can significantly reduce the amplitude of the unsteady lift force exerted on the body. When combined with low levels of base bleed, these perturbations can completely suppress the unsteadiness in the wake with reduced levels of mass injection in the flow.

1. Introduction

Suitable three-dimensional perturbations applied to nominally two-dimensional basic flows are known to be able to weaken and even suppress vortex shedding in the wake of bluff bodies (see, e.g., [1,2] and [3] for a review). It has recently been shown that this stabilizing action is associated with the quenching of the local absolute instability in the wake [4,5], leading to the stabilization of the associated global mode [6,7].

In the case of 3D control of 2D wakes, the role of the stabilizing perturbations is essentially to force spanwise periodic perturbations of the streamwise velocity in the wake. In the literature pertaining to wall-bounded shear flows, these spanwise periodic perturbations of the streamwise velocity are known as 'streamwise streaks' and they are known to be very efficiently forced by streamwise vortices through the lift-up effect (see, e.g., [8,9] for a review). The shape of the optimal forcing leading to the maximally amplified streaks can be computed through standard optimization techniques and is associated with large energy amplifications of the forcing, whose maximal value typically increases with the Reynolds number. Such an optimization has been recently performed on parallel and non-parallel model wakes [5,6] and on the circular cylinder wake [7], showing that the efficiency of the 3D control of 2D wakes can be greatly improved by forcing the streaks optimally. In the case of the cylinder 2D wake, it is found that the optimal spanwise wavelengths leading to the most amplified streaks in the wake almost coincide with the ones that are the most efficient to quench vortex shedding [7].

While important progress has been achieved in the case of the 3D control of nominally 2D wakes, the same is not true in the case of three-dimensional wakes, which are the most relevant to many applications (see, e.g., [10] for a discussion of this issue in the context of the aerodynamics of heavy vehicles). The scope of the present study is therefore to test

E-mail address: carlo.cossu@imft.fr (C. Cossu).

http://dx.doi.org/10.1016/j.crme.2017.05.010

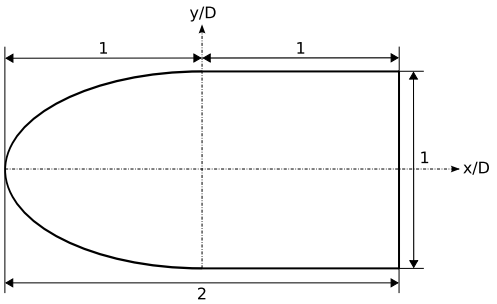

Fig. 1. Longitudinal section of the axisymmetric blunt-based cylinder of diameter D with axis x parallel to the free-stream velocity. The blunt nose of the cylinder is a half-ellipsoid of circular cross-section (diameter D) and longitudinal half-axis of length D extending from $x/D=-1$ to $x/D=0$. The tubular body has a diameter D and extends from $x/D=0$ to $x/D=1$.

the effectiveness of an extension to 3D wakes of the approach used for 2D wakes. We choose as a testbed the wake of a blunt-based axisymmetric bluff body with an ellipsoidal nose and a square back whose global stability has been previously investigated [11]. For this configuration, it has been found that the sequence of global instabilities developing in the wake is similar to the one observed for a sphere and in other axisymmetric wakes with a first steady instability of the axisymmetric wake that breaks the axisymmetry by giving rise to a non-zero steady lift force. This primary state then undergoes a (secondary) instability leading to unsteadiness in the wake and to an unsteady lift force on the body. It has also been shown that for the considered configuration these global instabilities can be stabilized with base bleed [11]. Our approach, similarly to previous investigations [5–7,12–15], consists in first computing the steady, azimuthally ('spanwise') periodic optimal perturbations inducing the maximum growth of streaks in the wake and then study their stabilizing effect on the wake unsteadiness. We anticipate that the found $m\neq 1$ optimal perturbations have a stabilizing effect on the global instabilities.

The mathematical formulation of the problem is introduced in §2. The computed optimal energy amplifications and the associated perturbations as well as the analysis of their stabilizing effect are presented in §3. These results are further discussed in §4 where some conclusions are also drawn.

2. Problem formulation

We consider the flow of an incompressible viscous fluid of density ρ and kinematic viscosity ν past an axisymmetric blunt-based cylinder of diameter D and total length $L=2D$ whose axis is parallel to the free-stream velocity $U_\infty \mathbf{e}_x$ (where $\mathbf{e}_x$ is the unit vector oriented parallel to the axis x of the cylinder). The blunt nose of the cylinder is an ellipsoid with circular cross-section of diameter D and longitudinal half-axis with 2:1 ratio. The tubular body has a diameter D and a length D (see Fig. 1). In dimensionless coordinates based on D, therefore, the nose of the body extends from $x=-1$ to $x=0$, the tubular body from $x=0$ to $x=1$, and the wake occupies the region $x>1$.

The flow is governed by the Navier–Stokes equations for an incompressible viscous fluid:

$$\nabla\cdot\mathbf{u}=0,\qquad \frac{\partial\mathbf{u}}{\partial t}+\mathbf{u}\cdot\nabla\mathbf{u}=-\nabla p+\frac{1}{Re}\nabla^2\mathbf{u} \tag{1}$$

where $\mathbf{u}$ and p and the dimensionless velocity and pressure fields and $Re=U_\infty D/\nu$ is the Reynolds number. The velocity, pressure, lengths and times have been made dimensionless with U_∞, ρU_∞^2, D and D/U_∞ respectively. Homogeneous boundary conditions for the velocity are enforced on the body surface except in the controlled case where wall-normal control velocities are enforced.

In the first part of the study, we compute the linear optimal spatial perturbations of the steady axisymmetric solution to the Navier–Stokes equations $\mathbf{U}_0$, which is linearly stable for sufficiently low Reynolds numbers. These perturbations satisfy the Navier–Stokes equations rewritten in perturbation form:

$$\nabla\cdot\mathbf{u}'=0,\qquad \frac{\partial\mathbf{u}'}{\partial t}+\mathbf{u}'\cdot\nabla\mathbf{U}+\mathbf{U}\cdot\nabla\mathbf{u}'+\mathbf{u}'\cdot\nabla\mathbf{u}'=-\nabla p'+\frac{1}{Re}\nabla^2\mathbf{u}' \tag{2}$$

where $\mathbf{U}=\mathbf{U}_0$ and the nonlinear term $\mathbf{u}'\cdot\nabla\mathbf{u}'$ is neglected for the computation of the linear optimal perturbations. In the following, steady perturbations $\mathbf{u}'$ are considered, which are of particular interest in open-loop flow control applications and which are forced by radial blowing or suction $u'_{\mathrm{w}}(\theta,x)\mathbf{e}_{\mathrm{r}}$ enforced on the body lateral surface ($0<x/D<1$, $r/D=1/2$). Similarly to [7], the optimal spatial energy amplification of wall control forcing is defined as $G(x)=\max_{u_{\mathrm{w}}} e'(x)/e'_{\mathrm{w}}$, where e'_{w} is the (input) kinetic energy of the blowing and suction forced on the lateral surface and e' is the (output) local perturbation kinetic energy at the station x respectively defined, in dimensionless coordinates, as $e'_{\mathrm{w}}=(1/4)\int_0^{2\pi}\int_0^1 (u'_{\mathrm{w}})^2\,\mathrm{d}x\,\mathrm{d}\theta$ and $e'(x)=(1/2)\int_0^{2\pi}\int_0^\infty \mathbf{u}'\cdot\mathbf{u}'\,r\,\mathrm{d}r\,\mathrm{d}\theta$.

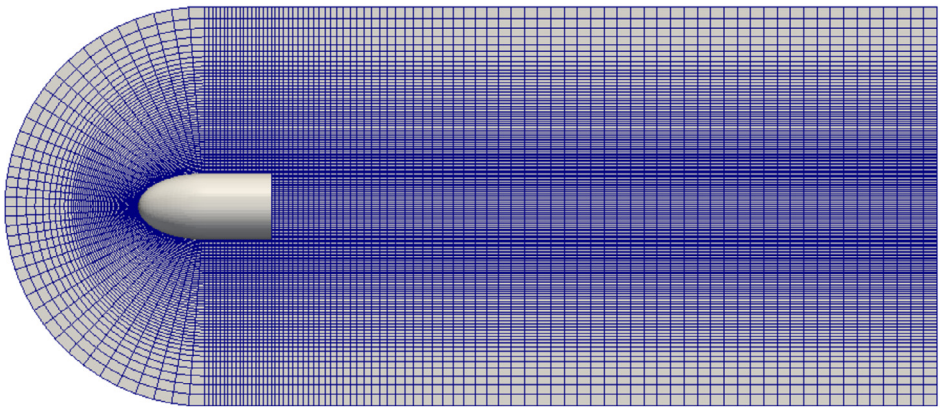

Fig. 2. Longitudinal section of the grid showing the increased grid density in the regions of higher shear.

To numerically compute $G(x)$ and the associated optimal wall perturbation, we follow an approach similar to the one recently applied to the circular cylinder wake [7]. The (control) radial velocity, enforced on the lateral cylindrical surface $u'_{\rm w}(\theta,x)$ is decomposed on a set of linearly independent functions $b_{\rm w}^{(n)}$, in practice truncated to N terms, as: $u'_{\rm w}(\theta,x)=\sum_{n=1}^{N} q_n b_{\rm w}^{(n)}(\theta,x)$. Denoting by $\mathbf{b}^{(n)}(\theta,r,x)$ the perturbation velocity field obtained by using $b_{\rm w}^{(n)}(\theta,x)$ as input, from linearity it follows that $\mathbf{u}'(\theta,r,x)=\sum_{n=1}^{N} q_n \mathbf{b}^{(n)}(\theta,r,x)$. The optimal energy growth can therefore be computed with its subspace approximation $G(x)=\max_{\mathbf{q}} \mathbf{q}^{\rm T}\mathbf{H}(x)\mathbf{q}/\mathbf{q}^{\rm T}\mathbf{H}_{\rm w}\mathbf{q}$, where $\mathbf{q}$ is the N-dimensional control vector of components q_n and the components of the symmetric matrices $\mathbf{H}(x)$ and $\mathbf{H}_{\rm w}$ are defined as $H_{nj}(x)=(1/2)\int_0^{\infty}\int_0^{2\pi}\mathbf{b}^{(n)}\cdot\mathbf{b}^{(j)} r\,{\rm d}\theta\,{\rm d}r$; $H_{w,mn}=(1/4)\int_0^{2\pi}\int_0^{1} b_{\rm w}^{(m)}(\theta,x)\,b_{\rm w}^{(n)}(\theta,x)\,{\rm d}\theta\,{\rm d}x$. The optimal energy growth $G(x)$ is easily found as the largest eigenvalue $\mu_{\max}$ of the generalized $N\times N$ eigenvalue problem $\mu\mathbf{H}_{\rm w}\mathbf{w}=\mathbf{H}\mathbf{w}$. The corresponding eigenvector $\mathbf{q}^{(\rm opt)}$ is the set of optimal coefficients maximizing the kinetic energy amplification at the selected streamwise station x, and the corresponding optimal blowing and suction is given by $u'^{(\rm opt)}_{\rm w}(\theta,x)=\sum_{n=1}^{N} q_n^{(\rm opt)} b_{\rm w}^{(n)}(\theta,x)$. In the following, as the basic flow $\mathbf{U}_0$ is axisymmetric and the equations linear, our results are obtained by computing independently the single-harmonic azimuthally periodic perturbations $u'_{\rm w}(\theta,x,m)=f(x)\cos m\theta$. The maximum growth is finally defined as $G_{\max}=\max_x G(x)$, and is separately computed for each considered azimuthal wavenumber and converged by increasing the truncation order N.

In the second part of the study, the effect of three-dimensional optimal perturbations on the wake unsteadiness is investigated by forcing them with finite amplitude $A_{\rm w}$, and therefore enforcing the following radial velocity at the wall in the nonlinear numerical simulations: $u'_{\rm w}(x,m)=A_{\rm w} f^{(\rm opt)}(x,m)\cos m\theta$, where $f^{(\rm opt)}$ is normalized so as to obtain $e'_{\rm w}=(\pi/2)A_{\rm w}^2$. The cost of the control can be quantified with the momentum coefficient of forcing $C_\mu=\left(\int_{S_{\rm lat}} u_{\rm w}^2{\rm d}S+\int_{S_{\rm base}} u_{\rm b}^2{\rm d}S\right)/(\pi R^2 U_\infty^2/2)$, which, using dimensionless units, is $C_\mu=8A_{\rm w}^2+2C_{\rm b}^2$. Even more importantly in applications, the cost of the control can also be quantified in terms of dimensionless mass flux $C_Q=\left(\int_{S_{\rm lat}} u_{\rm w}\,{\rm d}S+\int_{S_{\rm base}} u_{\rm b}\,{\rm d}S\right)/(\pi R^2 U_\infty)$. When optimal perturbations with $m>0$ are used, the associated mass flux is zero and therefore $C_Q=C_{\rm b}$. However, for $m=0$, the mass flux is non-zero and in this case, in dimensionless units $C_Q=C_{\rm b}+4A_{\rm w}\int_0^1 f^{(\rm opt)}(x,m=0)\,{\rm d}x$, where positive and negative $A_{\rm w}$ are associated with blowing and suction, respectively.

All the presented results are based on numerical integrations of the full or the linearized Navier–Stokes equations performed using a customized version of *OpenFoam*, an open-source finite volume code (see http://www.openfoam.org), which has already been validated and used in a series of previous investigations in our group [5–7]. The flow is solved in a three-dimensional domain extending $2.5\,D$ upstream of the body, $3\,D$ from the symmetry axis, and $10\,D$ downstream of the body stern. The grid is structured and refined near the body surface, as shown in Fig. 2. The PISO and SIMPLE algorithms have been respectively used to advance the solution in time and to compute steady solutions.

3. Results

The different regimes of the wake observed in the uncontrolled case (no normal velocity forced on the body surface) have been thoroughly investigated in [11]. A steady axisymmetric flow is observed for Reynolds numbers below $Re_1\simeq 319$. At $Re=Re_1$, the axisymmetry flow becomes globally unstable and is replaced by a steady flow characterized by the presence of two (steady) counter-rotating vortices originated in the near wake and that diffuse further downstream. This new steady flow becomes unstable at $Re_2\simeq 413$. Periodic vortex shedding is observed just above this second critical Reynolds number. Our numerical simulations retrieve these different regimes, as shown in Fig. 3 where the vortical structures corresponding to $Re=300$, $Re=350$, $Re=415$, and $Re=500$ are shown. The signatures of these different numerical regimes are well recognisable on the lift force exerted on the body, as shown in Fig. 4. While the lift is zero in the axisymmetric regime, it rises to a non-zero steady value in the range $Re_1<Re<Re_2$ and, for $Re>Re_2$, begins to oscillate around that non-zero

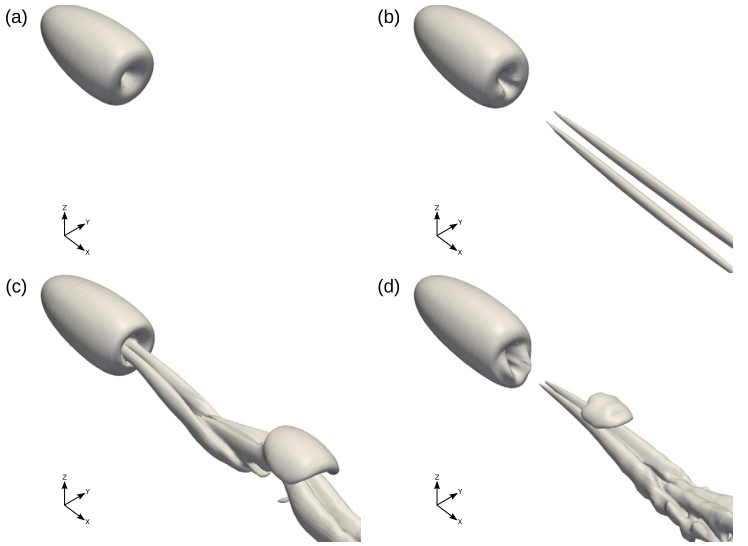

Fig. 3. Vortical structures on the surface and the wake of the bluff body in the uncontrolled case in different dynamical regimes visualised with the $Q = 0.001$ surfaces. (a) At $Re = 300$, the flow is steady and axisymmetric. (b) At $Re = 350$, a steady (non-axisymmetric) flow with two counter-rotating streamwise vortices in the wake is observed. (c) At $Re = 415$, a periodic global mode oscillates on top of the counter-rotating vortices, while (d) at $Re = 500$ additional structures of smaller scales and higher frequencies enter the picture.

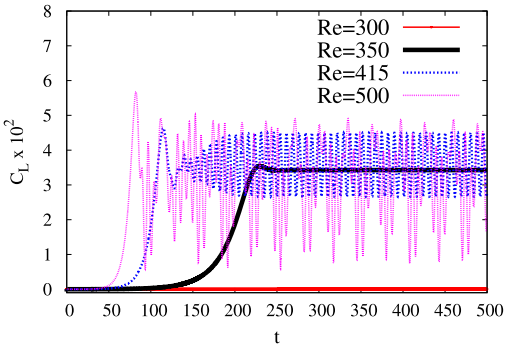

Fig. 4. Temporal history of the lift coefficient associated with the four dynamical regimes reported in Fig. 3. The permanent regime is observed for $t > \approx 250$. At $Re = 300$ the flow is steady and axisymmetric and therefore has zero lift. At $Re = 350$, the steady non-axisymmetric solution displays a steady lift which at $Re = 415$ oscillates periodically. A higher level of the oscillations and additional frequencies are observed at $Re = 500$.

mean value. The amplitude of the oscillations and their frequency content increase when the Reynolds number is further increased.

Having summarized the 'reference' uncontrolled dynamics of the wake, we next consider the optimal energy amplifications that can be supported by the axisymmetric wake steady solution $\mathbf{U}_0$. In the axisymmetric case, the optimal amplifications and the associated optimal perturbations can be separately computed for the different azimuthal wavenumbers. We therefore compute the optimal spatial amplification of the steady radial velocity forcing $u'_w(\theta, x, m) = f(x)\cos m\theta$ of azimuthal wavenumber m applied on the body lateral skin at $Re = 300 < Re_1$. Following the procedure described in §2, the streamwise distribution $f(x)$ for $0 < x < 1$ is approximated with an expansion on Chebyshev polynomials $T_n(\xi)$ (where $\xi = 2x - 1$) truncated to N terms. Similarly to what was found in previous studies [6,7], the optimal amplification is found to converge to a 1% precision with $N \sim O(10)$ terms, as shown in Fig. 5. The $m = 1$ mode is found to be the most amplified (with $G_{\max} > 500$). However, as this mode becomes linearly unstable (with a zero frequency) above the first critical Reynolds number Re_1 and therefore has a destabilizing action at higher Reynolds numbers, we do not further consider it in the following. The two most amplified modes at $Re = 300$ (excepted the $m = 1$) are the $m = 2$ and the $m = 0$, while the $m = 3$ and $m = 4$ are much less amplified, as shown in Fig. 6a. As expected, the amplifications increase with the Reynolds number (as shown in Fig. 6b for the $m = 2$ mode).

The dynamics of the $m = 0$ (axisymmetric) mode is qualitatively different from that of the other modes because, contrary to them: (a) it is not related to the amplification of streaks (the lift-up effect) but to the Orr mechanism [8], (b) it is associated with a non-zero mass flux, and (c) opposite effects are obtained with negative or positive amplitudes of u_w. This different behaviour is also recognisable on the longitudinal shapes $|f^{(\mathrm{opt})}|(x)$ of the optimal blowing and suction that are reported in Fig. 7. The shapes of the $m = 2$, $m = 3$ and $m = 4$ modes are very similar and they all correspond to

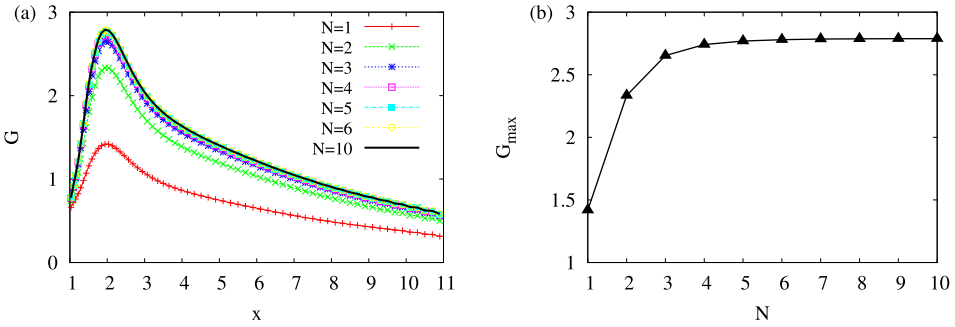

Fig. 5. (a) Convergence of the $G(x)$ optimal spatial energy growth curve with the number N of linearly independent distributions of wall blowing and suction included in the optimization basis for the $m = 2$ perturbations at $Re = 300$. (b) Corresponding convergence of the maximum amplification G_{max} with N. Converged results are obtained with $N \approx 6$ terms.

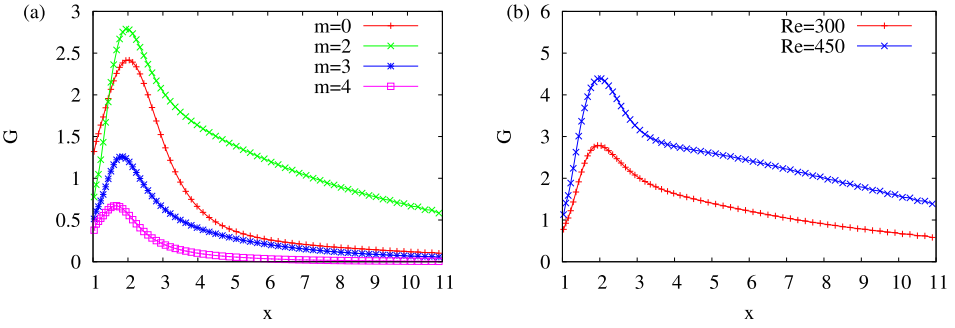

Fig. 6. Dependence of the optimal growth curve $G(x)$ on the azimuthal wavenumber m at $Re = 300$ (panel *a*) and on the Reynolds number for the $m = 2$ mode (panel *b*).

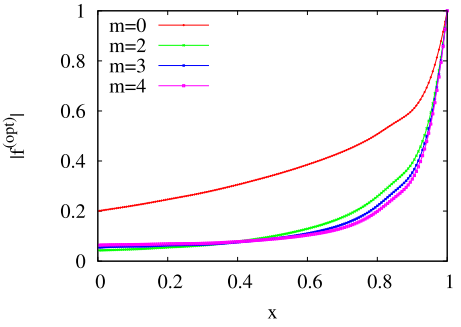

Fig. 7. Longitudinal shape $|f^{(opt)}|(x)$ of the optimal blowing and suction at $Re = 300$, where all the functions have been normalized by their maximum absolute value.

spanwise periodic blowing and suction increasingly concentrated near the trailing edge, while for the $m = 0$ mode the optimal distribution $|f^{(opt)}|(x)$ is non-negligible in the upstream half of the lateral section. The variations of $|f^{(opt)}|(x)$ with Re are small (not shown), similarly to what was found in the 2D case on the circular cylinder [7]. The spanwise periodic optimal blowing and suction of $m \neq 0$ modes induces counter-rotating streamwise vortices that decay downstream while forcing the growth of streamwise streaks, as shown in Fig. 8.

Having computed the optimal perturbations leading to the optimal energy growth in the wake, we next consider their effect on the unsteady wake for $Re > Re_2$. To this end, for each considered azimuthal mode $m \neq 1$, we select the shape of the optimal forcing leading to the maximum amplification G_{max} and we do force it with finite amplitude A_w. We find that this forcing has (for $m \neq 1$) a stabilizing effect on the unsteadiness of the wake as measured by variations of the lift coefficient C_L. For the $m = 0$ forcing the stabilizing effect is obtained with suction ($A_w < 0$), while blowing ($A_w > 0$) has the opposite effect (not shown). The effect of the forcing on the $C_L(t)$, shown in Fig. 9 for the $m = 2$ mode, is to lead to a permanent reduction of both the amplitude of the lift oscillations and their mean value when the amplitude A_w of optimal blowing and suction is increased. The stabilizing effect of forcing optimal perturbations is associated with an increasing 'symmetrization' of the wake induced by the forced streaks, as shown in Fig. 10.

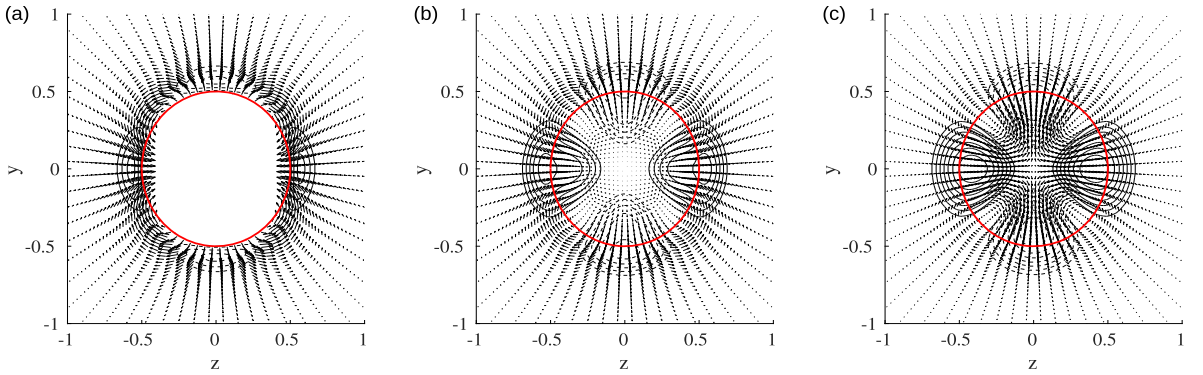

Fig. 8. Cross-stream ($y-z$) view of the velocity perturbations forced by the $m=2$ optimal blowing and suction at $Re=300$ at the three selected streamwise stations: $x=1$ (bluff-body stern, panel *a*), $x=(x_{\max}+1)/2$ (midway to the position of maximum streak amplitude, panel *b*) and $x=x_{\max}$ (position of maximum streak amplitude, panel *c*). The scales used to plot the cross-stream v'–w' velocity components (streamwise vortices, arrows) and the streamwise u' component (streamwise streaks, contour lines) are the same in all panels. The circular cross section of the base of the bluff body is also reported as a (red) circle for reference.

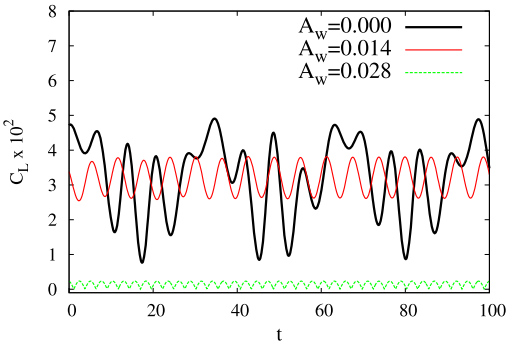

Fig. 9. Temporal history of the lift coefficient associated with the uncontrolled flow at $Re=500$ ($A_{\mathrm{w}}=0$, as also reported in Fig. 4) and with the increasing amplitudes A_{w} of the $m=2$ optimal blowing and suction at $Re=500$.

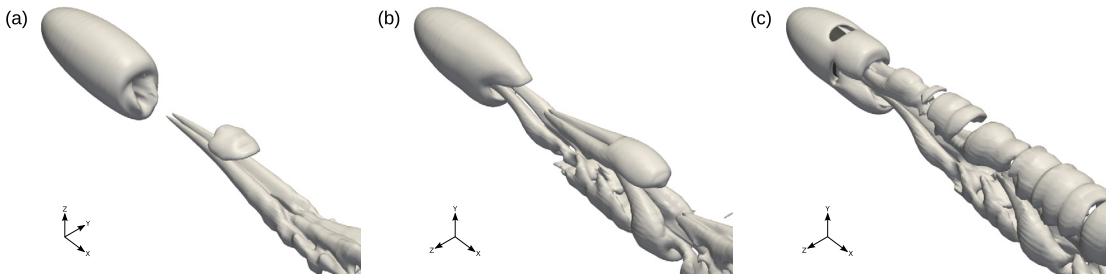

Fig. 10. Vortical structures (visualised with the $Q=0.001$ surfaces) on the surface and the wake of the bluff body at $Re=500$ in the uncontrolled case (panel *a*, which is the same as panel *d* of Fig. 3) and with the $m=2$ optimal blowing and suction enforced with $A_{\mathrm{w}}=0.014$ (panel *b*) and $A_{\mathrm{w}}=0.028$ (panel *c*).

Similar results are obtained for the other ($m\neq 1$) modes, as shown in Fig. 11, where the dependence of the root mean square amplitude of the lift coefficient oscillations $C_{\mathrm{L}}^{(\mathrm{rms})}$ on the control amplitude measured in terms of the momentum coefficient C_μ is reported. Complete stabilization can be obtained at $Re=415$ (near the critical Reynolds number) and significant reductions of the 'rms' amplitudes can be achieved at $Re=500$. However, excessive amplitudes of the control forcing can result in a new increase in $C_{\mathrm{L}}^{(\mathrm{rms})}$, now sustained by the induced streaks.

As already mentioned, for the considered flow, standard base bleed is an effective way to suppress unsteadiness in the wake [11]. We therefore compare the effect obtained with the selected azimuthal modes of optimal blowing and suction at $Re=500$ to the pure base bleed in Fig. 12a. From this figure, it is seen how, among the optimal blowing and suction controls, the least effective mode is the axisymmetric one $m=0$. The $m=2$ mode is the most effective at low forcing amplitudes, while $m=3$ is more effective at higher forcing amplitudes.

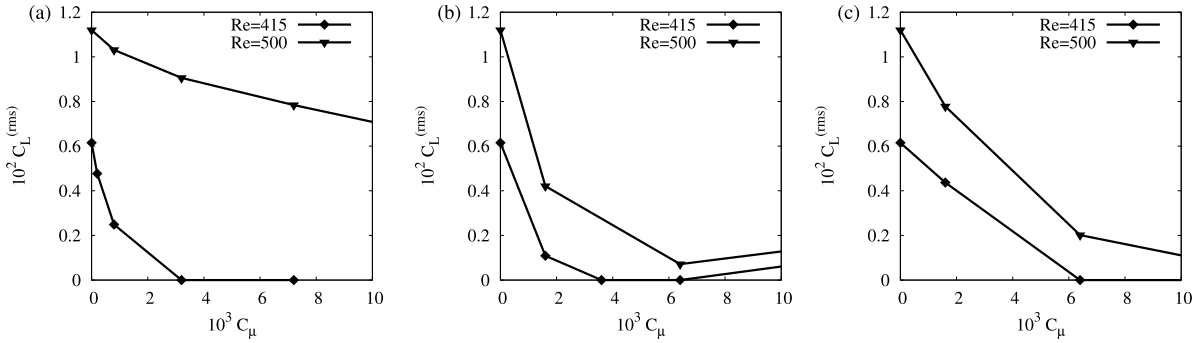

Fig. 11. Dependence of the $C_L^{(rms)}$ root mean square amplitude of the lift coefficient oscillation on the control amplitude measured in terms of the momentum coefficient C_μ for $Re = 415$ (diamonds) and $Re = 500$ (triangles) for the $m = 0$ (panel a), $m = 2$ (panel b) and $m = 3$ (panel c) optimal blowing and suction.

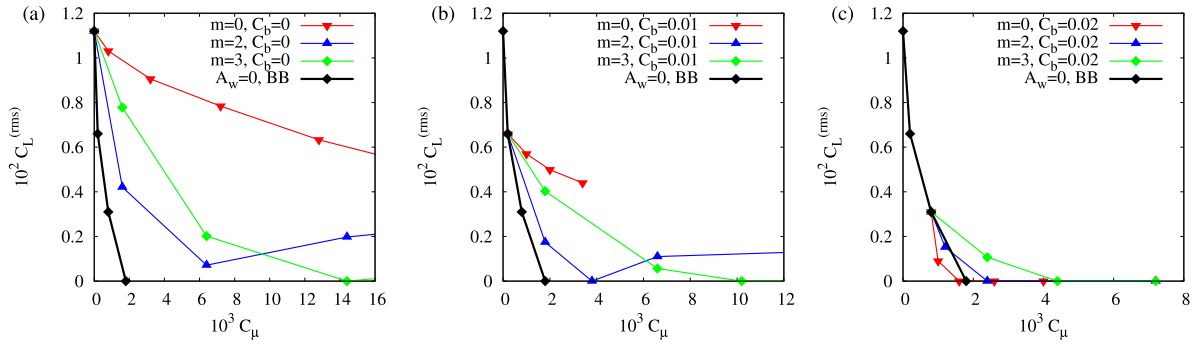

Fig. 12. Comparison of the $C_L^{(rms)}(C_\mu)$ dependence of the $m = 0$, $m = 2$ and $m = 3$ optimal blowing and suction in the absence of base bleed (panel a) and with base bleed $C_b = 0.01$ (panel b) and $C_b = 0.02$ (panel c). For convenience, these curves are compared, in all panels, to the one obtained by pure base bleed (BB) in the absence of any forcing of optimal blowing and suction ($A_w = 0$).

Pure base bleed ($A_w = 0$) is found to be more effective than the optimal blowing and suction, but at the cost of a steady mass injection in the flow (while $m \neq 0$ optimal blowing and suction are associated with zero mass flux). It is therefore interesting to test if combinations of base bleed and optimal blowing and suction could lead to the complete suppression of the unsteadiness using lower levels of mass injection in the wake. This is, actually, also interesting for the $m = 0$ mode, which, being associated with suction, could provide at least part of the mass used for base bleed. We have therefore explored if combinations of standard base bleed and optimal blowing and suction could enhance the control performance. The first two base bleed values reported in Fig. 12a ($C_b = 0.01$ and $C_b = 0.02$, corresponding to the second and third point from the right on the black-diamond curve) have therefore been used in combination with the optimal blowing and suction forcing, as reported in panels b and c of Fig. 12. From these figures, it is seen how the combination of optimal blowing and suction and base bleed is efficient, leading to the complete stabilization of the oscillations in the wake with a mass flux reduced when compared to the pure base bleed with the same C_μ.

4. Conclusions

The scope of this study was two-fold: (a) compute, for the first time, the optimal steady perturbations of a 3D (axisymmetric) wake induced by optimal blowing and suction on the skin of the body and (b) analyse if these optimal perturbations have a stabilizing effect on the wake when forced with finite amplitude. In its scope and methods, the present study is therefore an extension to 3D wakes of the approach successfully implemented on 2D wakes [6,7].

It is found that the steady ($m \neq 0$) optimal blowing and suction leads to the formation of streamwise vortices that induce the growth of streamwise streaks, like in 2D wakes. The $m = 1$ mode is the most amplified for $Re < Re_1$, but it becomes linearly unstable for $Re > Re_1$. Other modes are also amplified but, contrary to what found in 2D wakes, they are associated with maximum amplifications that are smaller than those found in the 2D case on the circular cylinder. This is not extremely surprising because, in the 2D circular cylinder wake, the most amplified mode corresponds to a spanwise wavelength $\lambda_z \approx 5 - 7\,D$ (where D is the cylinder diameter), while shorter wavelengths are much less amplified. As in the axisymmetric case, the analogous of the spanwise wavelength is $\lambda_z \approx \pi D/m$, the maximum accessible 'spanwise wavelengths' are therefore small, e.g., $\lambda_z/D \approx 1.5$ for $m = 2$. The maximum amplifications achievable in an axisymmetric wake are therefore arguably small if an analogy with the 2D wake is made. Another consequence of the relatively small accessible λ_z is that the streamwise position where the maximum growth is attained is also smaller than in the 2D case

at comparable Reynolds numbers. Similarly to 2D wakes, the longitudinal shape of the optimal blowing and suction is not sensitive to the azimuthal wavenumber m (except for the $m = 0$ mode whose amplification is based on a different mechanism).

We have also shown that, when forced with finite amplitude, $m \neq 1$ optimal blowing and suction has a stabilizing effect on the unsteadiness in the wake, reducing the mean and the fluctuating amplitude of the lift. When combined with the usual base bleed on the body base, this type of control can lead to the complete stabilization of the wake even at $Re = 500$. As the stabilizing optimal blowing and suction is associated with a zero mass flux for $m > 0$ and to net *suction* for $m = 0$, when combined with base bleed, the stabilization is obtained with smaller mass fluxes than in the pure base bleed case. Further investigation is under way to find if a combined optimisation including the base bleed shape can lead to further improvements of this control strategy.

Acknowledgement

Financial support from PSA Peugeot–Citroën is kindly acknowledged.

References

[1] M. Tanner, A method of reducing the base drag of wings with blunt trailing edges, Aeronaut. Q. 23 (1972) 15–23.
[2] P.W. Bearman, J.C. Owen, Reduction of bluff-body drag and suppression of vortex shedding by the introduction of wavy separation lines, J. Fluids Struct. 12 (1) (1998) 123–130.
[3] H. Choi, W.P. Jeon, J. Kim, Control of flow over a bluff body, Annu. Rev. Fluid Mech. 40 (2008) 113–139.
[4] Y. Hwang, J. Kim, H. Choi, Stabilization of absolute instability in spanwise wavy two-dimensional wakes, J. Fluid Mech. 727 (2013) 346–378.
[5] G. Del Guercio, C. Cossu, G. Pujals, Stabilizing effect of optimally amplified streaks in parallel wakes, J. Fluid Mech. 739 (2014) 37–56.
[6] G. Del Guercio, C. Cossu, G. Pujals, Optimal perturbations of non-parallel wakes and their stabilizing effect on the global instability, Phys. Fluids 26 (2014) 024110.
[7] G. Del Guercio, C. Cossu, G. Pujals, Optimal streaks in the circular cylinder wake and suppression of the global instability, J. Fluid Mech. 752 (2014) 572–588.
[8] P.J. Schmid, D.S. Henningson, Stability and Transition in Shear Flows, Springer, New York, 2001.
[9] L. Brandt, The lift-up effect: the linear mechanism behind transition and turbulence in shear flows, Eur. J. Mech. B, Fluids 47 (2014) 80–96.
[10] H. Choi, J. Lee, H. Park, Aerodynamics of heavy vehicles, Annu. Rev. Fluid Mech. 46 (1) (2014) 441–468.
[11] P. Bohorquez, E. Sanmiguel-Rojas, A. Sevilla, J.I. Jiménez-González, C. Martínez-Bazán, Stability and dynamics of the laminar wake past a slender blunt-based axisymmetric body, J. Fluid Mech. 676 (2011) 110–144.
[12] C. Cossu, L. Brandt, Stabilization of Tollmien–Schlichting waves by finite amplitude optimal streaks in the Blasius boundary layer, Phys. Fluids 14 (2002) L57–L60.
[13] C. Cossu, L. Brandt, On Tollmien–Schlichting waves in streaky boundary layers, Eur. J. Mech. B, Fluids 23 (2014) 815–833.
[14] G. Pujals, S. Depardon, C. Cossu, Drag reduction of a 3D bluff body using coherent streamwise streaks, Exp. Fluids 49 (5) (2010) 1085–1094.
[15] A.P. Willis, Y. Hwang, C. Cossu, Optimally amplified large-scale streaks and drag reduction in the turbulent pipe flow, Phys. Rev. E 82 (2010) 036321.